NORSAR Scientific Report No. 1-2004

Semiannual Technical Summary

1 July - 31 December 2003

Frode Ringdal (ed.)

Kjeller, February 2004

6.5 Study of regional variations of the coda characteristics in the Barents Sea using small-aperture arrays

6.5.1 Introduction and first observations

At regional distances, coda waves arriving after deterministic phases like Pn, Pg, Sn, or Lg, are broadly attributed to seismic wave scattering phenomena associated with heterogeneities located within the crust. Therefore, the characteristics of the coda depend on the characteristics of the seismic source, but also on the properties of the medium of propagation. The analysis of phases composing the coda are then ideally suited for studying crustal structures.

Detailed analyses of coda phases can be made by using small-aperture seismic arrays. Compared with a single station, seismic arrays give the advantage of recording spatio-temporal sampling of the seismic wavefield. Therefore, array analysis not only enhances the signal-to-noise ratio (SNR) to emphasize more details in the seismograms, but it also allows the association of phase velocities and backazimuths with the coherent arrivals of the seismograms.

In this study, our objective was to obtain a better understanding of the propagation effects that affect the seismic wave field when it propagates through the Barents Sea. This work was motivated by the particular characteristics (parameters of propagation) observed for the coda of an earthquake located in northern Norway (Lat 64.68° N; Lon 22.85° E) and recorded by the ARCES array. We performed frequency-wavenumber (f-k) analysis (Kværna & Doornbos, 1986) in a moving window to analyze the waveforms of all 25 vertical components recorded by ARCES. Fig. 6.5.1 shows the results that we obtained for this particular earthquake located northern Scandinavia. The signals are band-pass filtered in the most energetic (highest SNR) frequency band (here this frequency band is 2 – 8 Hz). We used a 2 s window length to perform the wavenumber decomposition. For each time window, the most energetic peak of the wavenumber decomposition is selected and the parameters of propagation (direction and apparent velocity) are deduced from its position in the wavenumber domain. The relative power of this main peak, which is actually a coherency measure of the waveforms over the whole array, is also calculated. Fig. 6.5.1c is a map of the studied area and the black dotted line shows the source-array propagation path for this earthquake. Fig. 6.5.1a shows the signal recorded by the central sensor of the array and Fig. 6.5.1b gives the time evolution of the parameters of propagation. For each time window, we present the difference between the observed direction of propagation obtained from the wavenumber decomposition and the theoretical backazimuth. The color scale gives a measure of the apparent velocities of the different phases observed, in this case between 2.5 and 8 km/s. The size of each dot is proportional to the coherency of the wavefield calculated within each time window. The velocity scale and the coherency scale are depicted on the right hand side of the picture.

For this earthquake, the regional Pn, Pg, Sn, and Lg phases are clearly identified. The directions of propagation are very close to the one expected and exhibit a high stability for the different time windows, from the first arrival until the beginning of the Lg-coda. The seismic waves that compose the Lg-coda are clearly characterized by larger scattering from the direction of propagation. The time evolution of the apparent velocities shows that the Pn-coda is essentially composed of Pn phases, the Sn-coda of Sn phases and the Lg-coda of Lg phases. One has also to notice the high coherency of the waveforms over the whole array, not only for the deterministic phases of the seismograms, but also for the time windows used for analyzing Pn- and Sn-coda.

The time-azimuth-velocity evolution obtained for this earthquake shows that the most important scattering processes arise along the direct epicenter-array path. Lateral heterogeneities of the medium seem not to be involved in the main scattering processes. Such features of the coda have already been observed by different authors and mechanisms like multiple refractions in the crust have been proposed to explain the coda characteristics similar to those observed for this particular earthquake (Vogfjord & Langston, 1989; Dainty & Toksöz, 1990; Baumgardt, 1990).

The strong stability and coherency of the coda phases observed for this event contradicts the model of a random process, which generally is used to explain the coda, and shows that some deterministic processes of scattering are also responsible for the coda. The objective of this study is to have a better overview of the physical processes that govern the coda formation in northern Norway and adjacent areas. Therefore, we selected around 50 seismic events located in and around the Barents Sea, in order to answer specific questions:

- Can the temporal stability of the directions of propagation be observed independently from the location of the earthquakes?
- Is there a variability of the nature (P/S) of the coda phases depending on the source-array propagation path?
- How are the coda characteristics modified when the events are recorded by other arrays?

6.5.2 The data set

We selected around 50 seismic events located in and around the Barents Sea. Depending on their geographical locations, we divided the data set into 4 different groups represented in Fig. 6.5.2. The groups **G1**, **G2**, **G3,** and **G4** are composed of events located along the **Mid-Atlantic ridge**, close to **Svalbard**, close to **Novaya Zemlya** and in the **northern Fennoscandia / Kola Peninsula Region** respectively. In this study, we mainly focused on the observations made by the two arrays ARCES (Mykkeltveit *et al.*, 1990) and SPITS (Mykkeltveit *et al.*, 1992; Fyen & Ringdal, 1993) on Spitsbergen in the Svalbard Archipelago (Fig. 6.5.2).

We applied the processing as described in the first section to each event of the data set in order to retrieve the time-frequency evolutions of the parameters of propagation of the different phases of the coda. This processing is mainly divided into two steps:

- Visual check of the data quality. We used as many sensors as available (ideally, this number is 25 for **ARCESS** and 9 for **SPITS**). The signals are band pass filtered in the frequency band corresponding to the highest SNR.
- F-k decompositions using the moving time window technique for the whole signals. This step gives the time evolution of the parameters of propagation of the different seismic phases that compose the seismograms. We used a fixed length for the time window, around 2 – 3 s, depending on the central frequency of analysis, *i.e.*, the applied band-pass filter.

6.5.3 The results

Comparison of the coda characteristics recorded by ARCES for all events belonging to group G4

In order to determine if the coda characteristics of the earthquake presented in Fig. 6.5.1 are similar for all the events located in northern Norway, we compared the time-evolution of the parameters of propagation that we obtained for all the events of group G4.

The results are presented in Fig. 6.5.3. This figure represents only the energetic distribution of the directions of propagation corresponding to the different phases that compose the coda. For each event, the energy of the incoming wavefield is summed up as a function of direction of propagation and we plot the results by using a polar representation. Each circle corresponds to a different event of group G4, and the red line points to the epicenter of the event.

First of all, we see that for each event, there is a very good agreement between the expected direction of propagation and the most energetic direction of the distribution. In addition, we observe a high sharpness of the distributions around their main peak. This characteristic shows a high temporal stability of the directions of propagation of the most energetic phases that contribute to the signal. Thus, this confirms that for the group of events located in the northern Fennoscandia / Kola Peninsula Region, the coda phases result mainly from multiple scattering along the direct source-array path. Scattering due to lateral heterogeneities along the great circle paths between the sources and ARCES is very weak.

Comparison of the coda characteristics recorded by ARCES for the different event groups (G1/G2/G3/G4)

We compared the typical coda characteristics that we obtained for the events of the group G4 (see Fig. 6.5.1) with the ones obtained for the events of the groups G1, G2 and G3. One typical event of each of these groups is represented in Fig. 6.5.4. On the right hand side, we plotted the direct propagation path for each of the 3 selected events and on the left hand side, we displayed the results of the f-k analysis.

For the events of the groups G2 and G3, we observe the same characteristics as for the one of group G4 presented in Fig. 6.5.1. The direction of propagation does not change greatly with time for these two events and is close to the expected receiver to source backazimuth. The apparent velocities follow the same pattern as for the event presented in Fig. 6.5.1 (Pn phases for Pn coda and Sn phases for Sn coda). In terms of wave composition, the strongest difference between the events of the group G4, and the events of the groups G2 and G3 (or more generally with all events for which a part of the propagation path lies within the Barents Sea) is the absence of Lg phases. The Lg blockage for events located in the Barents Sea and recorded by the ARCES array has been observed and investigated by several authors (Baumgardt, 2001; Hicks *et al.*, 2004).

The characteristics of the coda are completely different for the events belonging to the group G1, *i.e.*, the ones located along the Mid-Atlantic ridge. We observe that the Pn-coda is, in this case, not longer dominated by multiple Pn phases, but by phases characterized by lower velocities. In addition, the high temporal stability of the direction of propagation is no longer present and differences close to 50˚ between the observed and the theoretical backazimuth can now be observed. Another interesting feature is the deviation of the main direction of propagation in the Pn- and Sn-coda. The main Pn phase propagates through the array with the expected direc-

tion, but the coda phases exhibit a slow increase of the directions of propagation to more northern directions. The same pattern is observed for the S part of the seismograms. Such deviations have been quasi-systematically observed for all the events of group G1 and this result is summarized in the Fig. 6.5.5, where we represented the energetic distributions of the directions of propagation for all the events of this group. Compared with the energetic distribution calculated for the events of the group G4 (Fig. 6.5.3), we observe a widening of the distributions around the main peak. This means that the distributions of the direction of propagation of the coda phases are now much more scattered around the expected bachazimuth. Fig. 6.5.5 also shows that the main peaks of the distributions can show a systematic deviation from the expected direction of propagation. These deviations cannot be attributed to heterogeneities located close to the array since they are generally not observed for the events from the other groups (Fig. 6.5.3), even for events at similar azimuths.

These results are summarized on the map represented in Fig. 6.5.6. We separate the events that we will call *'normal events'* for which the Pn- and Sn-coda are composed of phases propagating with typical velocities values of Pn and Sn respectively, from the events called *'abnormal events'* which do not show this pattern. The locations of the normal and abnormal events are represented by red and black stars respectively in Fig. 6.5.6. With very few exceptions, the abnormal events are the events of the group G1, located along the Mid-Atlantic ridge, as the events of the groups G2, G3 and G4 exhibit a normal distribution of the coda phases. It is interesting to see that for the events of the group G3, the single event which does not conform to the normal distribution of coda phases is the nuclear explosion that took place in Novaya Zemlya on 24 October 1990.

Comparison of the coda characteristics at ARCES and at SPITS

We the processed the waveforms recorded by the SPITS array for some of the events of our data set (the ones with highest SNR). The processing procedure is the same as for the ARCES array, except that the SPITS array consists of 9 vertical sensors, instead of 25 for ARCES. In Fig. 6.5.7, the time-evolution of the parameters of propagation is shown for the same earthquake, for which the observation at ARCES is presented in Fig. 6.5.4b. The coda is characterized by even more stable parameters of propagation compared with the coda recorded by ARCES for this event. In addition, the coherency of the wavefield over the whole array (measured by the size of the dots) is higher for the waveforms recorded by SPITS than for the ones recorded by ARCES. To simulate a SPITS type array, the ARCES data were also processed for only 9 sensors. The result of this test was that configuration and smaller aperture of the SPITS array can be ruled out as reason for the observed, more coherent coda.

The more interesting events recorded by SPITS are the one located along the Mid-Atlantic ridge. For these events, two general situations are observed: (1) no S phase is observed or (2) when a S phase is observed, the coherency is very low or inexistent. The situation (1) is depicted in Fig. 6.5.8a, where we present the time evolution of the parameters of propagation for an event located along the Mid-Atlantic ridge and recorded at SPITS. For comparison, we present also the results for an event of group G2, approximately located at the same distance (Fig. 6.5.8b) from the array. For the event of the group G1, the time arrival of the S phase should be around 115 s but the results of the f-k decomposition does not exhibit any S-type energy. Instead, the velocities of propagation are very high, closer to typical Pn phases. These features may be partly related to the radiation pattern of the seismic source, but the complex structures located between the source and the array may also be responsible for a part of the

observed characteristics. The source mechanism of the earthquakes of group G1 should be investigated more carefully in order to find out, which of the two effects (source or propagation) is predominant.

6.5.4 Conclusion

We investigated the characteristics of the coda for a large data set recorded by ARCES and SPITS. F-k decompositions have been used to calculate the time evolution of the parameters of propagation of the different phases that compose the coda.

We show that for the arrays ARCES and SPITS, the characteristics of the coda are very similar for events located in northern Fennoscandia / Kola Peninsula region (G4), close to Novaya Zemlya (G3) and close to Spitsbergen in the Barents Sea (G2). The coda propagates mainly along the great circle paths between source and arrays. The apparent velocities are typical of Pn phases for the Pn coda and Sn phases for the Sn coda. In this case, we imply mechanisms like multiple crustal reflections to explain our observations.

The characteristics of the coda are very different for all the events of group G1, located along the Mid-Atlantic ridge. Strong differences are generally observed between the direction of propagation of the coda phases and the expected one. This shows that the scattering is no longer confined to the great circle path, but that lateral structures are also involved into multipathing and diffraction processes. In addition, compared with the events of the groups G2, G3 and G4, for which the Pn coda is mostly composed of Pn waves, the Pn coda of the events located along the Mid-Atlantic ridge are composed of energy travelling with lower apparent velocity, which is closer to typical Sn phase velocities. Such particular characteristics are observed both at ARCES and SPITS. One of the main differences between the wavefield propagation of the events of group G1, compared to the groups G2, G3 and G4 is that for the events located along the Mid-Atlantic ridge, the wavefield propagates across the western continental margin, characterized by strong topography of the Moho and a complex geometry. The continental margin is also known for many lateral heterogeneous geological features in the whole crust related with the opening of the North Atlantic (*e.g.*, Faleide, 2000). The P-to-S conversions and the backazimuth deviations that we observed for the events located along the ridge could be explained by the interactions with this large-scale structure. As further work, we plan to use the converted P-to-S travel time as well as the direction of propagation given by the array analysis in order to obtain a better characterization of the heterogeneous structures responsible for our observations.

Acknowledgements

The 3-month research term of ES at NORSAR in 2003 was funded through the EC programme Access to Research Infrastructure-project (Contract HPRI-CT-2002-00189).

Estelle Schissele, Institut für Geowissenschaften, Universität Potsdam, Germany
Johannes Schweitzer

References

Baumgardt, D. R. (1990). Investigation of teleseismic Lg blockage and scattering using regional arrays. Bull. Seis. Soc. Am. **80**, 2261-2281.

Baumgardt, D. R. (2001). Sedimentary basins and the blockage of Lg wave propagation in the continents. Pure Applied Geophysics **158**, 1207-1250.

Dainty, A. M. & M. N. Toksöz (1990). Array analysis of seismic scattering. Bull. Seis. Soc. Am. **80**, 2242-2260.

Faleide, J. I. (2000). Crustal structure of the Barents Sea – important constraints for regional seismic velocity and travel-time models. NORSAR Sci. Rep. **2-1999/2000**, 119-129.

Fyen, J & F. Ringdal (1993). Initial processing results for the Spitsbergen small-aperture array. NORSAR Sci. Rep. **2-92/93**, 119-131.

Hicks, E. C., T. Kværna, S. Mykkeltveit, J. Schweitzer & F. Ringdal (2004). Travel-times and attenuation relations for regional phases in the Barents Sea region. Pure appl. Geophys. **161**, 1-19.

Kværna, T. & D. J. Doornbos (1986). An integrated approach to slowness analysis with arrays and three-component stations. NORSAR Sci. Rep. **2-85/86**, 60-69.

Mykkeltveit, S., F. Ringdal, T. Kværna & R. W. Alewine (1990). Application of regional arrays in seismic verification. Bull. Seis. Soc. Am. **80**, 1777-1800.

Mykkeltveit, S., A. Dahle, J. Fyen, T. Kværna, P. W. Larsen, R. Paulsen, F. Ringdal & I. Kuzmin (1992). Extensions of the northern Europe regional array network – new small-aperture arrays at Apatity, Russia, and on the Arctic Island of Spitsbergen. NORSAR Sci. Rep. **1-92/93**, 58-71.

Vogfjord, K. S. and Langston, C. A. (1989) Multiple crustal phases from regional events recorded at NORESS. 11th Annual DARPA/AFGL Research Symposium, Proceedings, 466-473.

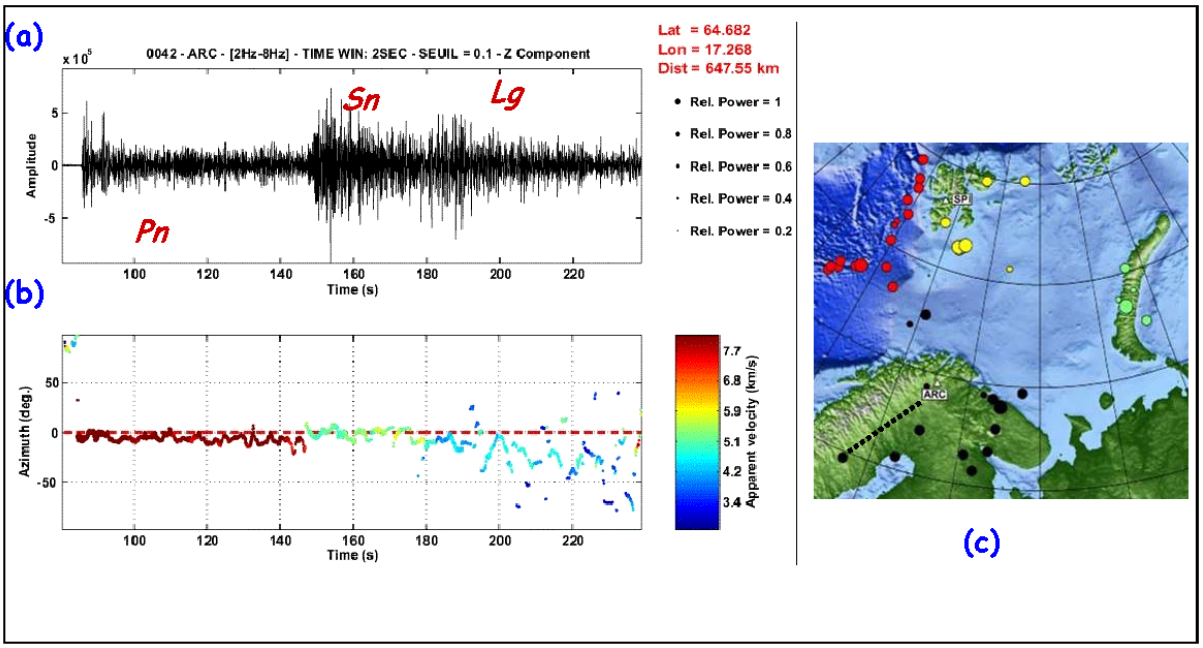

Fig. 6.5.1. *(a) Signal recorded by the central sensor of the ARCES array and band-pass filtered between 2 and 8 Hz. (b) Time-evolution of the directions of propagation. The color of each dot represents the apparent velocity obtained from the wavenumber decomposition and its size is a measure of the coherency of the waveforms over the whole array (measure between 0 and 1). The scales corresponding to the coherency and the apparent velocity are given on the right side of the figure. (c) Map of the studied area. The black black line shows the propagation path for this particular event.*

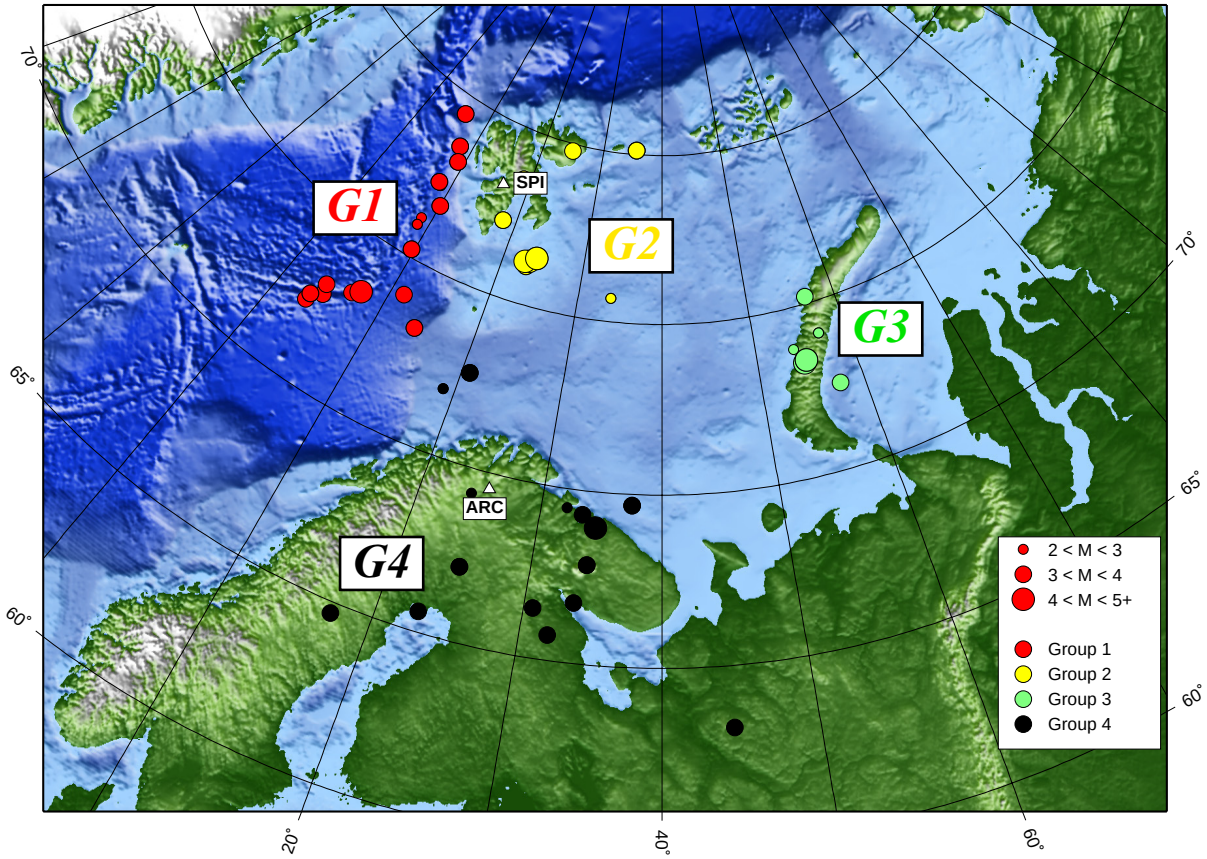

Fig. 6.5.2. *This map shows the location of the 4 groups of events (G1/G2/G3/G4) analyzed during this study. The size of each dot is proportional to the magnitude of the event.*

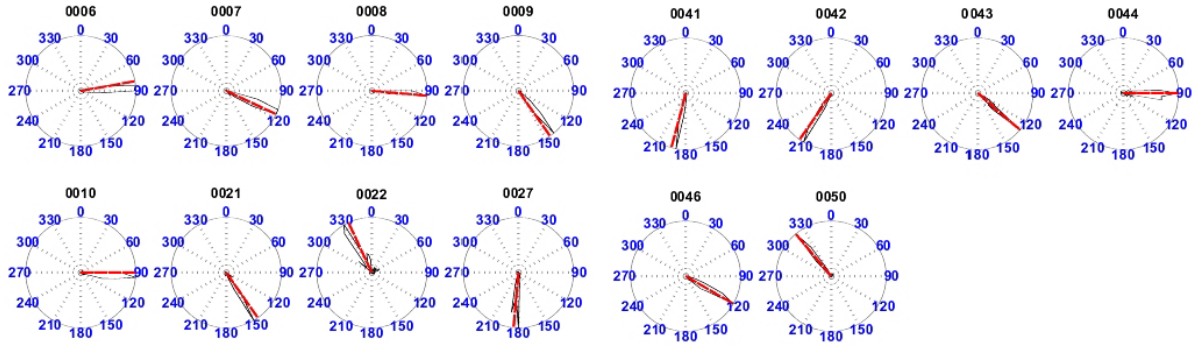

Fig. 6.5.3. *Energetic distributions of the directions of propagation for all the events of group G4 observed at ARCES.*

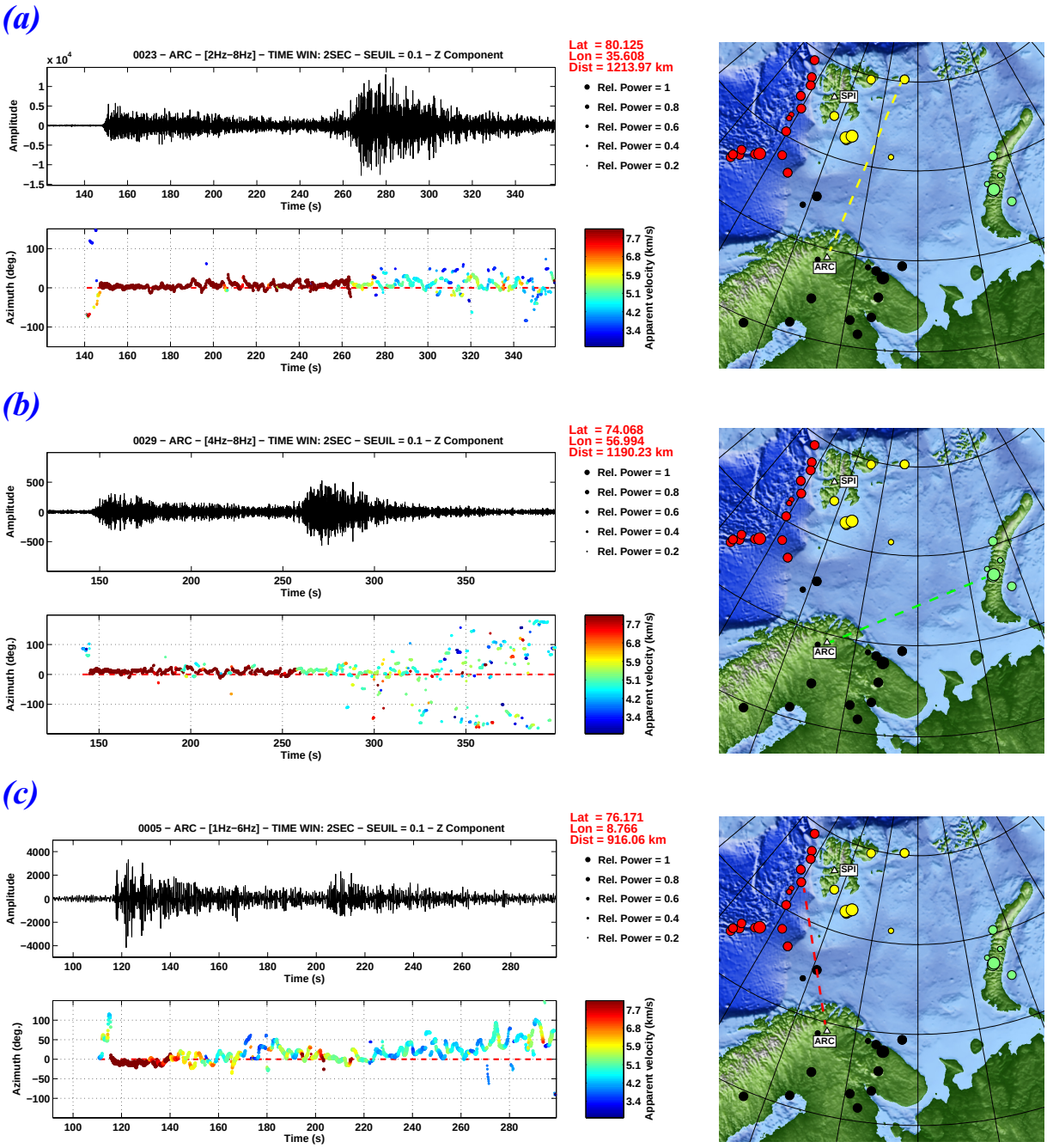

Fig. 6.5.4. *(a) Typical time evolution of the parameters of propagation for an event of group G2 observed at ARCES. (b) Idem for an event of group G3. (c) Idem for an event of group G1.On the right hand side, the propagation paths for the 3 events considered are represented.*

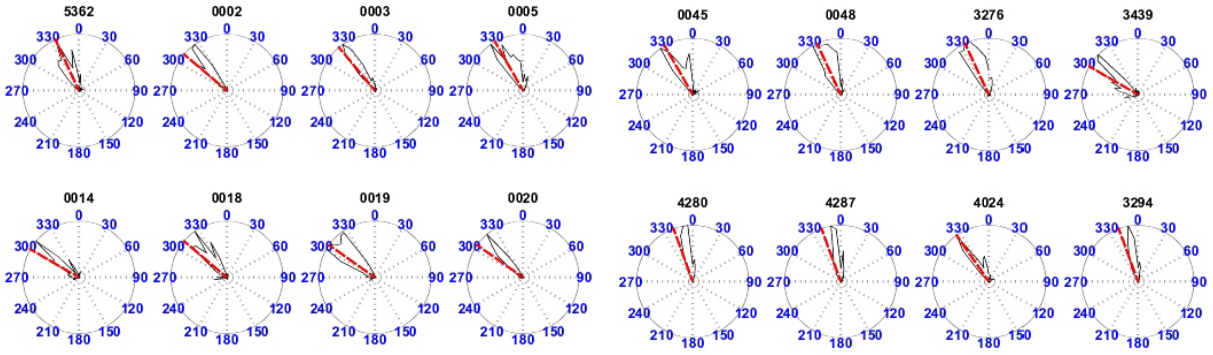

Fig. 6.5.5. *Energetic distributions of the directions of propagation for all the events of the group G1 observed at ARCES.*

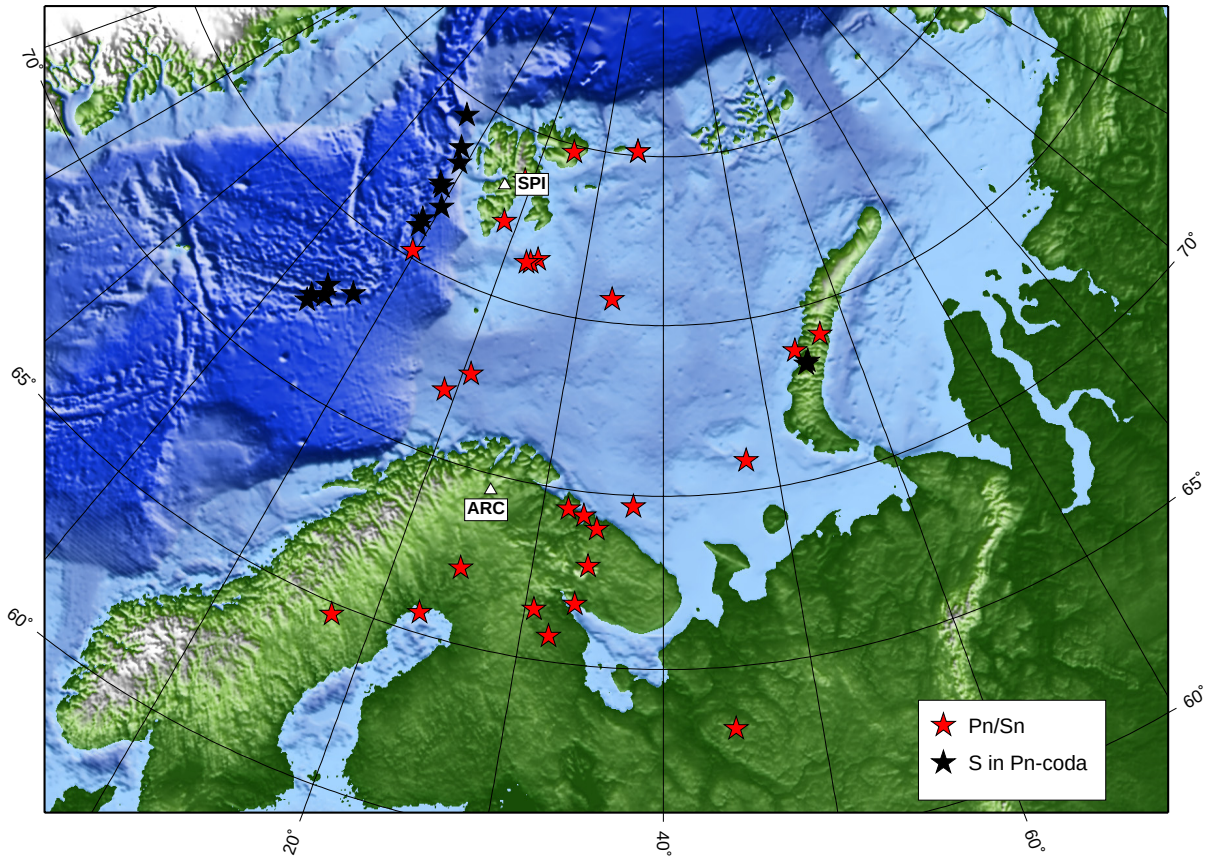

Fig. 6.5.6. *The red stars give the locations of the 'normal events' and the black stars give the locations of the 'abnormal events' (for details see text).*

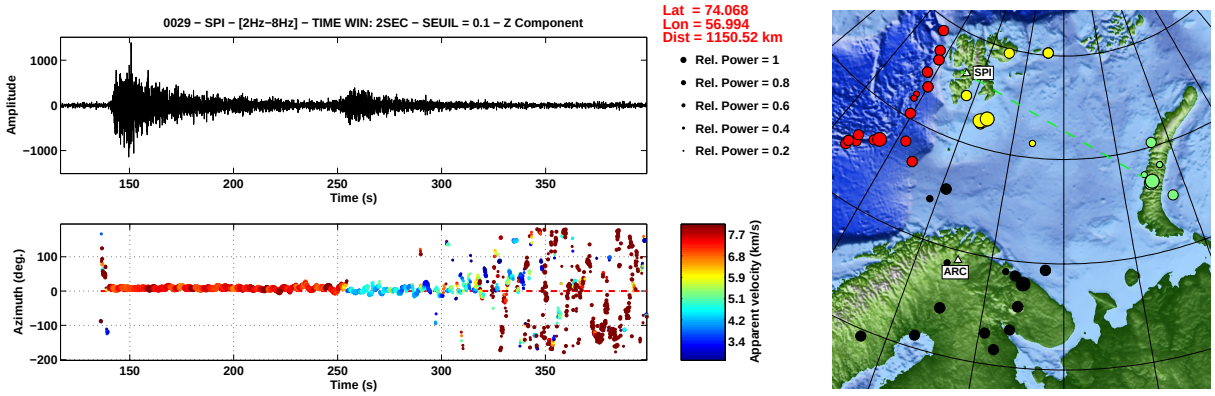

Fig. 6.5.7. *Time evolution of the parameters of propagation for an event of group G3 recorded at SPITS.*

(a)

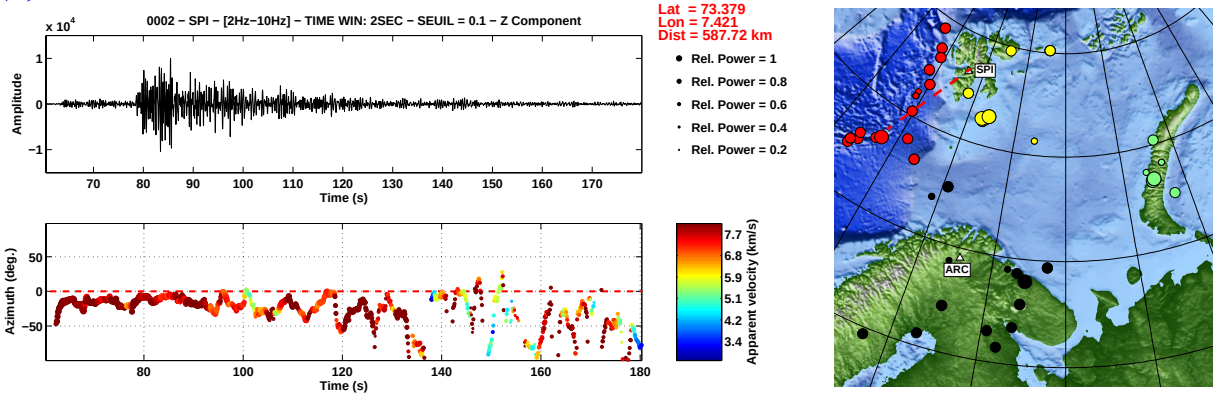

(b)

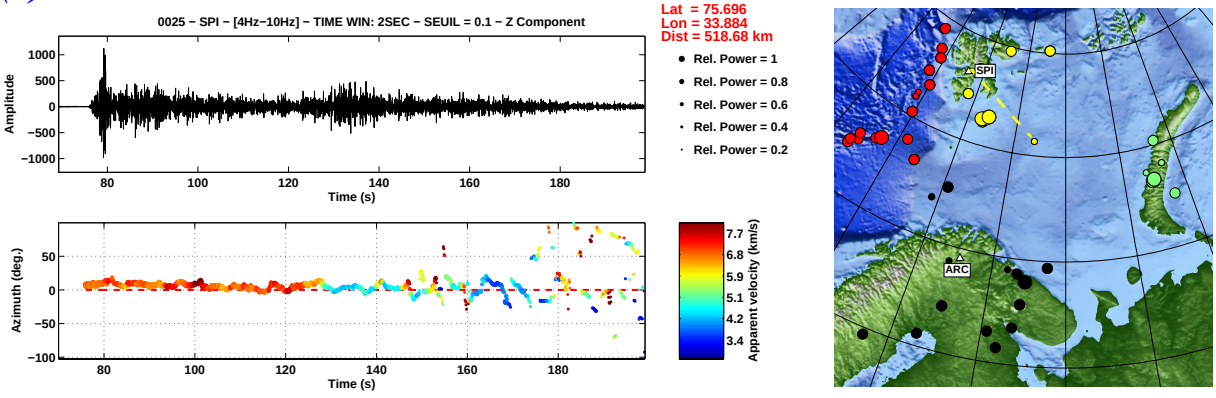

Fig. 6.5.8. *(a) Time evolution of the parameters of propagation for an event of group G1 recorded at SPITS. (b) Idem for an event of group G2.*